Science of the Total Environment 892 (2023) 164691

Contents lists available at ScienceDirect

Science of the Total Environment

journal homepage: www.elsevier.com/locate/scitotenv

Enhanced daytime atmospheric mercury in the marine boundary layer in the South Oceans

Yi Tang [a,e], Qingru Wu [a,b,*], Shuxiao Wang [a,b,*], Min Zhang [c], Yanxu Zhang [d], Fangli Qiao [c]

[a] State Key Joint Laboratory of Environmental Simulation and Pollution Control, School of Environment, Tsinghua University, Beijing 100084, China
[b] State Environmental Protection Key Laboratory of Sources and Control of Air Pollution Complex, Beijing 100084, China
[c] First Institute of Oceanography and Key Laboratory of Marine Sciences and Numerical Modelling, Ministry of Natural Resources, Qingdao 266061, China
[d] Joint International Research Laboratory of Atmospheric and Earth System Sciences, School of Atmospheric Sciences, Nanjing University, Nanjing 210023, China
[e] State Key Laboratory of Environmental Criteria and Risk Assessment, Chinese Research Academy of Environmental Science, Beijing 100012, China

HIGHLIGHTS

- Significantly elevated TGM during daytime was discovered in the Southern Hemisphere in the round-the-world cruise measurement.
- The elevated TGM was driven by surface oceanic Hg^{II} photoreduction.
- The diurnal amplitude of TGM might be impacted by the microbial productivity and the ratio of ultraviolet radiation.

GRAPHICAL ABSTRACT

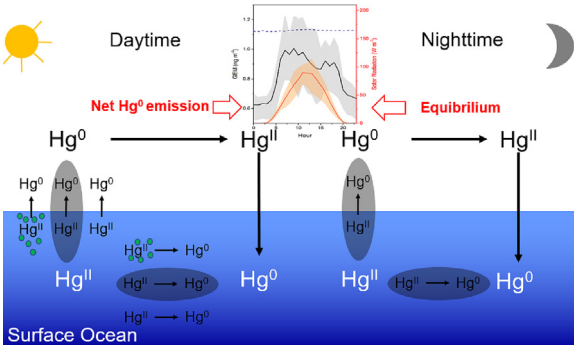

ARTICLE INFO

Editor: Xinbin Feng

Keywords:
Round-the-world cruise
Atmospheric mercury
Diurnal patterns
Photoreduction
South Oceans

ABSTRACT

Understanding the spatial and temporal variations of atmospheric mercury (Hg) in the marine boundary layer could advance our knowledge on ocean evasion of Hg. Here, we conducted continuous measurements of total gaseous mercury (TGM) in the marine boundary layer during a round-the-world cruise from August 2017 to May 2018. We observed the highest and lowest TGM concentrations in Southern Indian Ocean (1.29 ± 0.22 ng m^{-3}) and Southern Atlantic Ocean (0.61 ± 0.28 ng m^{-3}), respectively. During the daytime, enhanced TGM was observed with the diurnal amplitude difference reaching its maximum in the range of 0.30–0.37 ng m^{-3} in Southern Indian Ocean and Southern Ocean. The positive correlation between TGM (R^2 = 0.68–0.92) and hourly solar radiation in each ocean suggested that the daytime enhanced TGM was likely driven by Hg photoreduction in seawater, after excluding the influence of other meteorological factors. The diurnal amplitude of TGM in the marine boundary layer might be impacted by the microbial productivity and the ratio of ultraviolet radiation. Our study highlights that ocean acts as a net TGM source during the daytime in the Southern Hemisphere and aqueous photoreduction process may play an important role in the biogeochemical cycling of Hg.

1. Introduction

Mercury (Hg) is viewed as a toxic and global pollutant due to its biotoxicity and neurotoxicity (Ariya et al., 2015). Hg has long atmospheric lifetime, allowing it to be transported globally. In addition to the primary emission, Hg is re-emitted from terrestrial and oceanic surface to atmosphere (Driscoll et al., 2013). A large portion of anthropogenic Hg emissions would ultimately deposit into ocean (Amos et al., 2013; Gustin

* Corresponding authors at: State Key Joint Laboratory of Environmental Simulation and Pollution Control, School of Environment, Tsinghua University, Beijing 100084, China.
E-mail addresses: qrwu@tsinghua.edu.cn (Q. Wu), shxwang@tsinghua.edu.cn (S. Wang).

http://dx.doi.org/10.1016/j.scitotenv.2023.164691
Received 27 March 2023; Received in revised form 3 June 2023; Accepted 3 June 2023
Available online 8 June 2023

et al., 2020). Thus, the re-emission from the surface ocean plays an important role in the global biogeochemical cycling of Hg.

The diurnal pattern of atmospheric Hg in the boundary layer is controlled by short-term balances between emission, re-emission, oxidation, and deposition processes. For example, the TGM concentration reach its maximum during the nighttime and minimum during the daytime in the polar region, indicating rapid oxidation of TGM by bromine species and subsequent atmospheric Hg deposition (Wang et al., 2019). Previous studies have shown that terrestrial observation sites exhibited pronounced diurnal variation, with a daytime peak in urban areas and a nighttime peak in rural areas due to anthropogenic emissions and changes of boundary layer height. However, studies on the marine boundary layer (MBL) have shown no dominant diurnal variation (Fu et al., 2015; Lan et al., 2012; Mao et al., 2016), with most studies conducted in the northern hemisphere (Mao et al., 2016). In the southern hemisphere, atmospheric Hg measurements only available at several observation stations such as Cape Point, Amsterdam Island and some limited ocean area such as Southern Ocean and south Pacific Ocean (Angot et al., 2014, 2016; Martin et al., 2017; Soerensen et al., 2014; Wang et al., 2017). As a result, the diurnal characteristic of atmospheric Hg in the MBL of southern hemisphere is especially unclear, and a global map of atmospheric Hg variation is necessary to illustrate the role of the ocean on global Hg cycling.

To better understand the diurnal pattern of Hg in the MBL and the impact of oceanic Hg emission, we conducted measurements of total gaseous mercury (TGM) during a round-the-world cruise from August 2017 to May 2018. Then, we examined the diurnal pattern of TGM, its magnitude difference between daytime and nighttime. In addition, we investigate the driving processes of diurnal variation, and analyzed the factors that could influence the photoreduction process, such as meteorological conditions (including solar radiation, wind speed, and temperature) and net primary production (NPP). By synergistic analyzing observational and remote sensing data, we aim to identify the characteristics of TGM in MBL and discover the driving factors of TGM variation.

2. Methodology

2.1. Sampling sites

The Measurements were conducted at a cruise vessel known as "R/V Xiangyanghong 01" by the First Institute of Oceanography, Ministry of Natural Resources of China. The instruments were installed above the bridge at the starboard railing at the R/V deck of the ship to avoid the direct contamination from the ship exhaust (about 20 m above the sea level) (Fig. S1). The voyage started from Qingdao, China, crossed the Southern Indian Ocean and Southern Atlantic Ocean via the Cape Town, South Africa and then Punta Arenas, Chile. After completing the Antarctic scientific research, the ship crossed the Pacific Ocean via Papeete Port, France and finally returned to Qingdao, China. The detailed cruise route and period were shown in Fig. 1. To reduce the interference of terrestrial processes, we only selected the cruise data 150 km away from the continent and divided the cruise tracks into 4 parts: Southern Ocean (55°S–62°S, 37°W–65°W), Pacific Ocean (53°S–10°N, 70°W–180°W), south Atlantic Ocean (26°S–52°S, 60°W–20°E) and south Indian Ocean (24°S–27°S, 33°E–56°E).

2.2. Atmospheric hg measurements

The TGM were measured by a Tekran 2537× mercury vapor analyzer (Tekran Inc., Toronto, Canada), which was calibrated in every 25 h with an internal calibration source. The sampling interval was 5 min, with a sampling flow rate of 1.0 L min^{-1}. The detection limit was 0.1 ng m^{-3} and systematic uncertainty was 10 % (Slemr et al., 2015). A Teflon filter holder was installed prior to air inlet to filter sea salt and other particles and minimize the influence of wind speed and wind direction. The soda lime was replaced once a week to remove the water vapor of humid air. According to previous studies, we assume that the gaseous oxidized mercury (GOM) in humid air of MBL would be filtered out together with PM at PTFE filter and inlet tubing (Lyman et al., 2020). Thus, our observed data is comparable with the gaseous elemental mercury (GEM) or TGM of other studies in MBL (Slemr et al., 2015). To avoid the impact of ship emissions on the sampling inlet, the TGM data were removed when the TGM exceeded the 90th percentile, and wind speeds were <2 m/s or wind direction deviated by <30° from the vessel's heading.

2.3. Ancillary data & data process

2.3.1. Meteorological data

Meteorological data including temperature (T), wind speed (WS), pressure and wind direction were provided by meteorological station during the cruise. The time resolution of meteorological station was 1 min. The data were averaged on an hourly basis for analysis.

2.3.2. Satellite data

Hourly shortwave radiation was extracted from the NASA's Clouds and Earth's Radiant Energy System (CERES) project (https://ceres.larc.nasa.gov/, last access: June 2023), which provides hourly all-sky surface spectral shortwave down flux with 1° × 1° resolution (Su et al., 2005). The ultraviolet dose data was obtained from Tropospheric Emission Monitoring Internet Service (TEMIS) (https://www.temis.nl/ last access: June 2023).

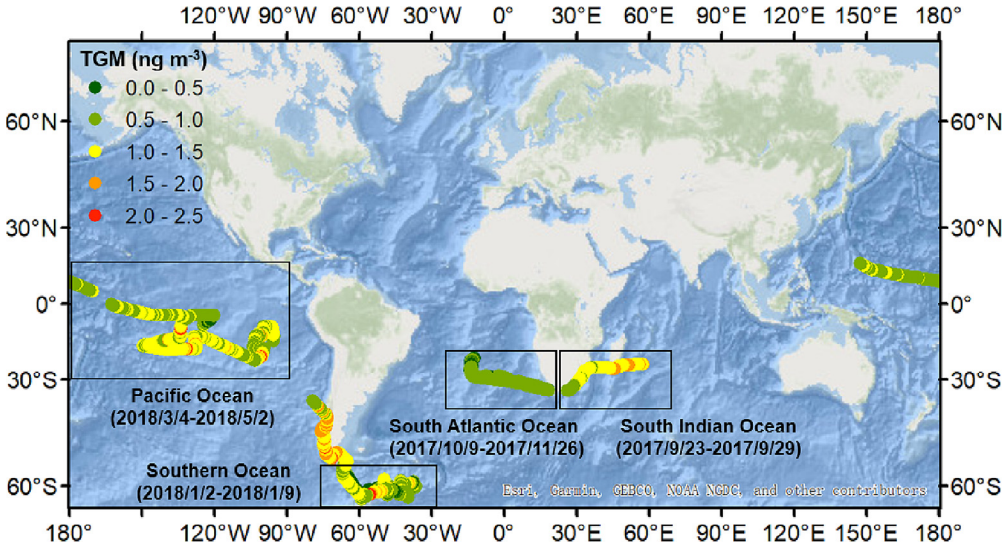

Fig. 1. Cruise Routine and hourly TGM concentration during the sampling campaign.

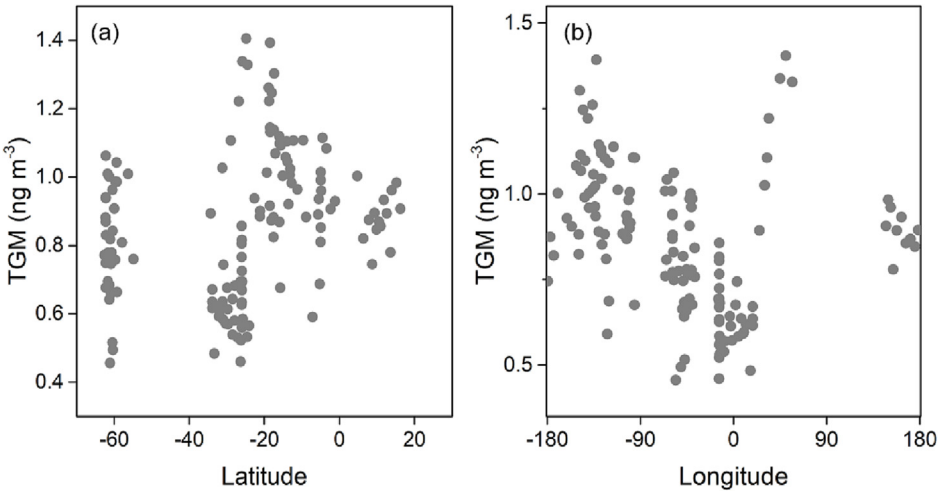

Fig. 2. The (a) latitudinal and (b) longitudinal difference of TGM during the cruise.

The NPP was calculated using Chlorophyll a (Chla) and temperature (Behrenfeld and Falkowski, 1997). The Chla data were estimated through satellite sensing data of ocean surface color using MODIS and AQUA. The detailed calculation method could be obtained by Hu et al., 2012. The Chla product was provided by NASA freely (https://neo.sci.gsfc.nasa.gov/, last access: June 2023). The specific Chla concentration was extracted from the 0.25° × 0.25° grid results based on the location and time of the cruise.

2.3.3. Trajectory data

To identify the potential source regions and understand the impact of air mass on TGM, we conducted backward trajectories during the cruise according to the previous studies (Kalinchuk et al., 2018a; Weiss-Penzias et al., 2013; Yue et al., 2022). The air mass trajectories was calculated by the Hybrid Single Particle Lagrangian Integrated Trajectory (HYSPLIT) model, with 1.0° × 1.0° gridded meteorological data from the Global Data Assimilation System (GDAS) (Polissar et al., 2001). The uncertainties of trajectories increased with time along the path (Fleming et al., 2012). Here, the total run time of backward trajectories was set to 72 h after considering precise potential source area and acceptable trajectories uncertainties (Stein et al., 2015). Considering that the ending point constantly changed during cruise, the calculation starting time was set 12:00 in local time zone every day to represent the backward trajectory that day and avoid confusion due to excessive trajectories. The ending point was set at 100 m above the sea level of the cruise location. All the backward trajectories were calculated by using MeteoInfo 10.2 (Tang et al., 2018).

2.3.4. Correlation analysis

Considering the geographical differences of TGM could interfere with the identification of the drivers on diurnal variation. We used the real-time diurnal normalized parameters to identify the effects of different factors on the diurnal variation of TGM. The detailed calculation method was as follows.

$$K_{normal} = K_t - K_{ave\ -\ 24\ h}$$

where K_{normal}, K_t, and $K_{ave\text{-}24h}$ were the diurnal normalized variable, variable at current hour and 24-h sliding average of this variable, respectively.

3. Results and discussion

3.1. Spatial variations of atmospheric hg

During the cruise campaign, hourly TGM concentrations in the MBL varied from 0.41 to 1.98 ng m^{-3} (N = 3381). The regional-averaged TGM concentrations were 1.29 ± 0.22 ng m^{-3} (South Indian Ocean), 0.80 ± 0.26 ng m^{-3} (Southern Ocean), 1.02 ± 0.24 ng m^{-3} (Pacific Ocean) and 0.61 ± 0.28 ng m^{-3} (South Atlantic Ocean), respectively (Fig. 2). Limited by the cruise conditions, there were only a few atmospheric Hg observations in MBL of southern hemisphere. The TGM measurement in this study expanded the global TGM observation dataset for these regions.

The TGM concentrations observed in this study were comparable with limited observational stations in the southern hemisphere from the Global Mercury Observation Systems and some cruise measurements, such as Cape point (1.10 ng m^{-3}), Andean Patagonia (0.86 ± 0.16 ng m^{-3}), Amsterdam (1.03 ± 0.08 ng m^{-3}), southern Pacific (0.78–0.86 ng m^{-3}) and southern Pacific (0.75 ± 0.13 ng m^{-3}) (Angot et al., 2014; Diéguez et al., 2019; Kuss et al., 2011; Yue et al., 2021, 2022), but lower than the polluted regions such as Chacaltaya (1.34 ± 0.01 ng m^{-3}) and background stations in the northern hemisphere (1.3–1.5 ng m^{-3}) (Koenig et al., 2021; Sprovieri et al., 2016). The longitudinal distribution showed the TGM reached lowest at 0° longitude (at South Atlantic Ocean), which is far away from the continents in southern hemisphere (Fig. 2b). The latitudinal distribution of TGM displayed a gradual increase from southern hemisphere to northern hemisphere (Fig. 2a). The latitudinal difference during the cruise indicates that less impact of anthropogenic emissions on the atmospheric Hg in the MBL of the southern hemisphere.

3.2. Temporal variations of atmospheric Hg

During the entire cruise, we find that TGM at 12:00 am local time was higher than that at 00:00 am in 118 out of the 133 complete daily data (Fig. S2). The averaged diurnal amplitude (the amplitude is defined as the concentration difference between TGM at 12:00 am and TGM at 00:00 am) was 0.12 ± 0.20 ng m^{-3} with the maximum daily diurnal amplitude of 0.58 ng m^{-3} occurred on Jan 16, 2018 in the Southern Ocean (Fig. S3). The diurnal pattern of TGM concentrations was similar across all ocean regions, characterized by a daytime increase starting from 5:00 to 6:00 am and reaching its maximum at approximately 12:00 pm (Fig. 3). Then, TGM concentrations began to decrease in the afternoon, remaining stable during the nighttime until sunrise the following day.

Although almost all measurements of this cruise exhibited pronounced diurnal variations (Fig. S4, Table S1) (Weiss-Penzias et al., 2013), the amplitude of diurnal variations varied significantly (t-test, $p < 0.01$) across different oceans. The highest amplitude was observed at the Indian Ocean (0.37 ± 0.14 ng m^{-3}) and the Southern Ocean (0.30 ± 0.33 ng m^{-3}), whereas the Southern Atlantic and the Southern Pacific had lower amplitudes of 0.09 ± 0.17 ng m^{-3} and 0.09 ± 0.08 ng m^{-3}, respectively. The cruise measurement in the South China Sea showed pronounced diurnal variation of TGM in spring, summer and autumn with the amplitude in

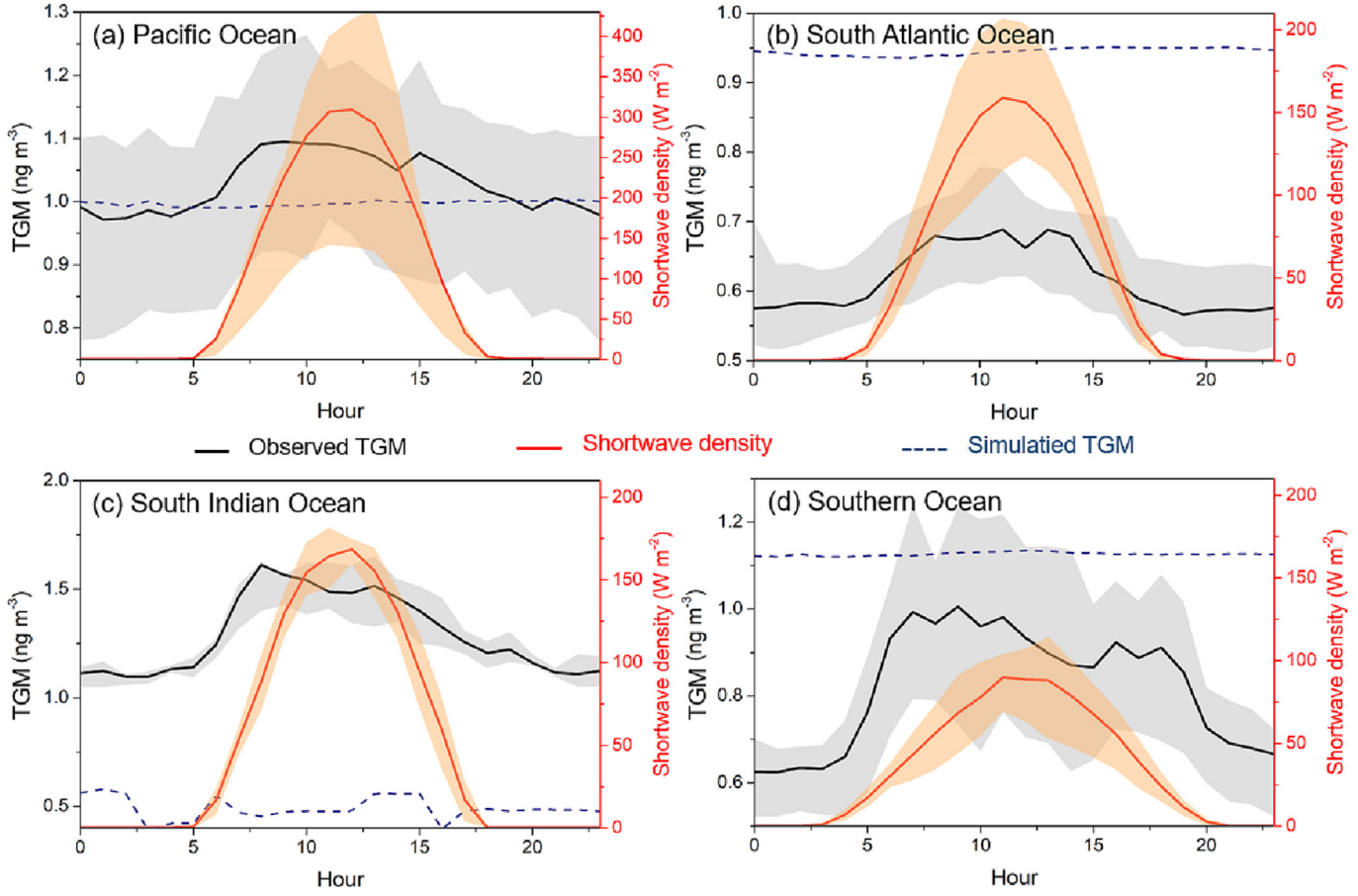

Fig. 3. The diurnal variation of TGM and shortwave radiation density in different oceanic areas during the sampling campaign (a) Pacific Ocean (55°S–62°S, 37°W–65°W); (b) South Atlantic Ocean (53°S–10°N, 70°W–180°W); (c) Southern Indian Ocean (26°S–52°S, 60°W–20°E); and (d) Southern Ocean (24°S–27°S, 33°E–56°E). The bold lines represent averaged value and the shaded areas were the 25th to 75th percentiles. The dot line were the hourly mean TGM concentration extracted from GEOS-Chem model used in Zhang et al. (2019).

the range of 0.80–1.00 ng m^{-3}, which was attributed to the potential ocean evasion (Tseng et al., 2012). In the remote oceanic areas, most diurnal pattern of TGM varied in the range of 0.00–0.14 ng m^{-3} (Kalinchuk et al., 2018b, 2019; Nerentorp Mastromonaco et al., 2016), similar with our results in the South Atlantic Ocean and the South Pacific Ocean. The diurnal amplitude of the Southern Ocean and the Southern Indian Ocean observed in this study were much higher than other observations in remote MBL, which is unexpected according to the latest global chemical transport model (Zhang et al., 2019), suggesting a primary or secondary source of Hg in these cruise parts.

3.3. Daytime enhancement of TGM induced by photoreduction

Generally, the increase in TGM can be attributed to a variety of factors including anthropogenic and natural emissions, meteorological events, and physics/chemical processes. During the cruise observations, there were no direct anthropogenic Hg emission sources or natural emissions (such as volcanic eruptions and wild fire), because the air mass in most of our observation sites were originated from the ocean based on backward trajectories (Fig. S5). Earlier studies have shown that in coastal areas of the Antarctic plateau, sunlight-induced melting of sea ice can rapidly release Hg from snow into the atmosphere (Angot et al., 2016; Dommergue et al., 2003). Our cruise in the Southern Ocean did not encounter the Antarctic ice sheet, which was located 100 km away from the ship. Moreover, the temperature, relative humidity, and wind direction have not exhibited significant diurnal variation, indicating that the airmass remains stable during both day and night. Therefore, the sea ice melting was not the dominant factor for TGM. Based on the meteorological data, there were no pronounced diurnal meteorological events (such as convection and cyclone) during the cruise (Fig. S2). Thus, the physics/chemical induced oceanic emission was the main potential driver of TGM during the daytime.

The wind speed and temperature could enhance oceanic TGM emission due to pressure difference of Hg between water and atmosphere based on Henry's Law (Andersson et al., 2008). However, the correlation analysis between the normalized diurnal TGM and meteorological parameters in each ocean indicates a low relationship between TGM and wind speed, as well as temperature (Fig. 4), which suggested that the elevated TGM levels observed during the daytime were not primarily driven by the air-sea exchange induced by meteorological parameters.

As reported by many lab experiments and field observation studies, the aqueous oxidized mercury (Hg^{II}) could be reduced to Hg^0 and released to atmosphere through diffusion processes (O'Driscoll et al., 2006; Qureshi et al., 2010). Given that solar radiation (including UV-A and UV-B) is the most important driver of Hg^{II} photoreduction in aqueous environment (Rose et al., 2015), we analyzed the correlation analysis between TGM and meteorological parameters. The diurnal normalized TGM only had relatively significant correlation (r = 0.21– 0.78, $p < 0.01$) with solar radiation (Fig. 4). Such positive correlation demonstrated that the photoreduction induced by solar radiation is probably an important factor for diurnal variation of TGM.

To differentiate the dominating driving forcing of TGM, we compared hourly average TGM with the shortwave radiation in each ocean regions (Fig. S6). We found that significant correlation (R^2 = 0.68–0.92, $p < 0.01$) between diurnal mean TGM and solar radiation at these four

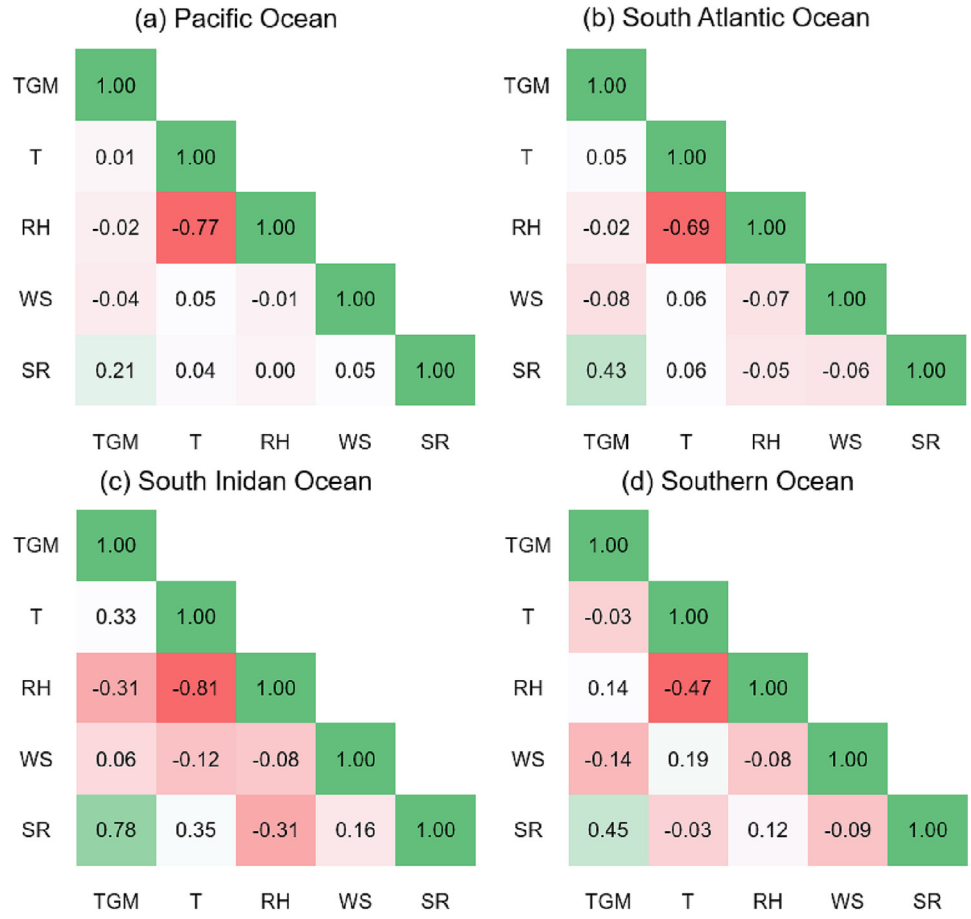

Fig. 4. Correlation analysis matrix for the real-time diurnal normalized variables and TGM concentrations in the MBL for the whole observational period (a) Pacific Ocean; (b) South Atlantic Ocean; (c) South Indian Ocean; (d) Southern Ocean.

oceanic parts. The correlation between TGM and shortwave radiation were strongest at the South Atlantic Ocean ($R^2 = 0.92$) and weakest ($R^2 = 0.68$) in the Southern Ocean. We noticed that the correlation coefficient based on hourly average data was much higher than the real-time hourly normalized data in a day ($r = 0.21$–0.78), indicating that diurnal variation of individual day was affected by the complex marine environment, including sea waves and variations in the boundary layer height. The analysis of average hourly data could reduce the effects of individual errors of TGM. The strong correlations between TGM and shortwave radiation demonstrate that the photoreduction of Hg^{II} can quickly occur in the ambient environment and dominant the diurnal variation of TGM.

The chemical reduction of Hg^{II} in the ocean involves both photochemical transformation and dark production (Kuss et al., 2015), leading to different diurnal variations across ocean regions. We found that the NPP has strong correlation with the TGM amplitude in global cruise measurement (Fig. 5). The strong correlation between NPP and the TGM amplitude could be potentially attributed to the following parameters. Firstly, the crucial factor that affect the diurnal variation was the photoreduction process. Secondly, the elevated NPP means the enhancement of the marine biological activities, which may contribute to the combination of dissolved organic carbon and Hg^{II} and result in enhanced microbe-mediated photoreduction (Siciliano et al., 2002). Meanwhile, other physical and chemical parameters, such as DOC and THg, remain relatively stable in those areas (Fig. S7). Despite we observed such high correlation coefficient between NPP and diurnal variation, the chemical photoreduction process is largely complicated and subject to various influencing factors apart from NPP. Therefore, further robust observation data is required to support this hypothesis.

Moreover, we noticed a relatively high diurnal amplitude of Hg in the Southern Ocean despite the relatively low NPP and solar radiation (Fig. 3, Fig. 5). The UV radiation reach up to 20 % of total solar radiation (60 W m^{-2}) in the Antarctica region (Zheng and Cheng, 2020) (Table S2), which was higher than the middle and low latitudes region (9.5 %–15.5 % during our cruise) (Williamson et al., 2014). Compared to the visible light, the UV light contains more energy and can promote the Hg^{II} reduction. The enhanced ratio of UV light ratio may accelerate the reaction rate of photoreduction, contributing to increased reduction of Hg^{II} to Hg^0 and subsequent release into the atmosphere (Qureshi et al., 2010; Yang et al., 2019).

4. Summary and implications

We carried out TGM measurements in a round-the-world cruise from August 2017 to May 2018 mainly in the South Oceans and found pronounced diurnal variations with peak values during the daytime in the MBL. The amplitude of diurnal variation reached 0.30 ± 0.33 ng m^{-3} in the Southern Ocean during summer, which was about 31 % of TGM concentration in Southern Ocean and higher than most previous observations in the MBL. By multiple factors correlations analysis, the diurnal amplitude of atmospheric Hg in the MBL was mainly driven by the Hg^{II} photoreduction while NPP and UV radiation would impact diurnal amplitude. Currently, global chemical transport models do not consider the impact of biological activity and solar radiation bands on reduction rates, resulting in an inability to simulate diurnal differences among oceans. The pronounced diurnal variation of TGM provided valuable data for the global atmosphere and ocean Hg model validation and revision in the future.

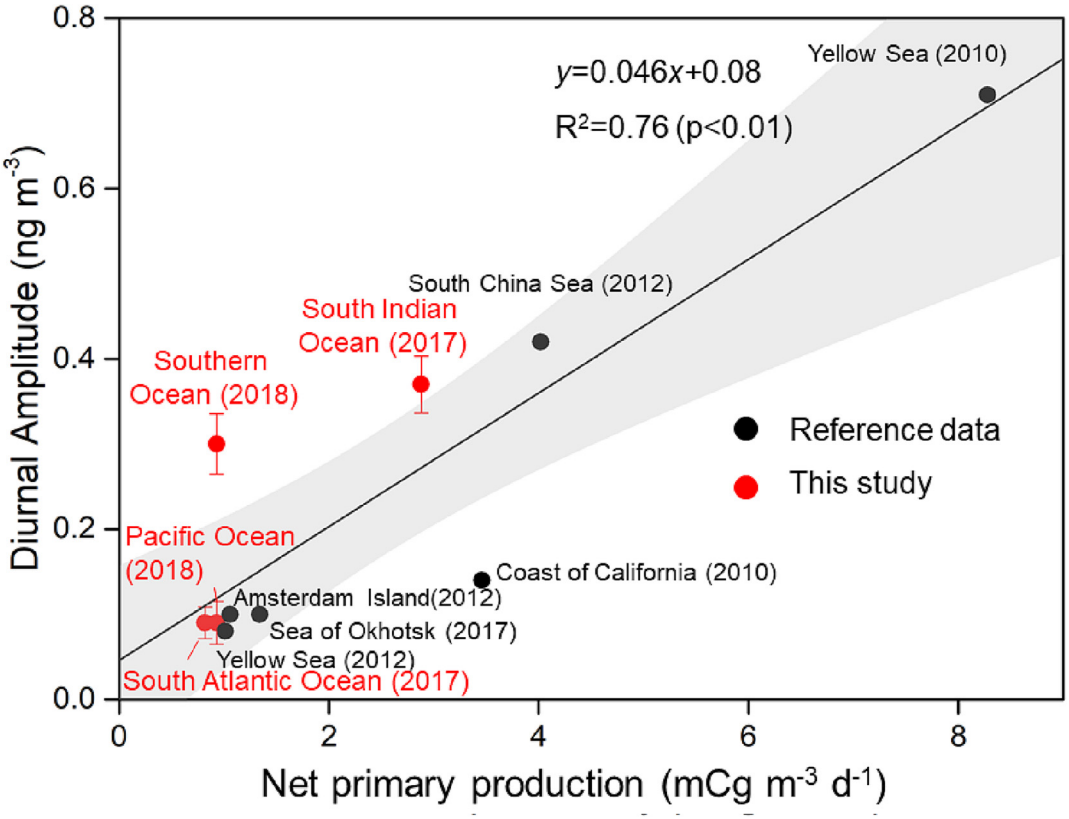

Fig. 5. Relationship between diurnal TGM amplitude and NPP. The data was extracted from our study and references (Angot et al., 2014; Ci et al., 2011, 2015; Kalinchuk et al., 2019; Tseng et al., 2012; Weiss-Penzias et al., 2013), and the number in brackets was the sampling year.

Based on our study, the major process that governs the cycle of atmospheric Hg in marine boundary layer is depicted in Fig. 6. During the nighttime, the mixing layer and atmospheric Hg remain stable, which indicated the weak photochemical and physical process (Angot et al., 2016; Wang et al., 2016). During the daytime, the aqueous Hg^{II} would be reduced to TGM and released to the atmosphere, which means that the ocean acted as a net TGM source during the daytime in the South Hemisphere. More experiments on Hg photoreduction should be conducted to quantitatively understand the oceanic emission rate in the MBL and the role of ocean in global Hg cycling. In addition, considering atmospheric Hg has decreased in the recent years (Wang et al., 2023; Zhang et al., 2016), continuous measurement of atmospheric Hg in ocean is needed to further quantitatively understand the role of oceanic emission on atmospheric Hg variations.

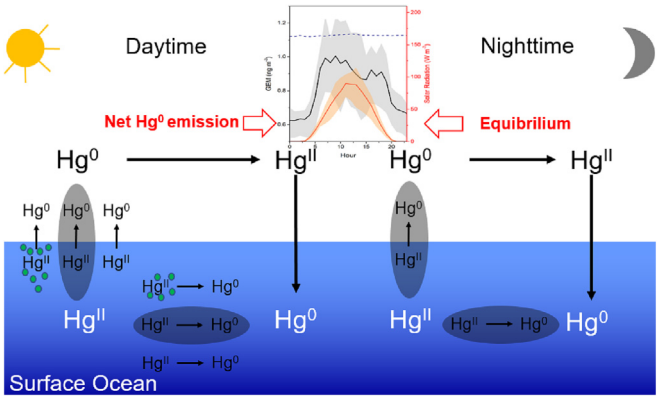

Fig. 6. A conceptual model showing the major processes that contributed to the diurnal pattern of TGM in marine boundary layer.

CRediT authorship contribution statement

Q.W., Y.T., S.W. and F.Q. designed the research. Y.T. and M.Z. performed the research. Y.T. and Q.W. analyzed the data. Y.Z. provided GEOS-Chem model data. Y.T., Q.W and S.W. wrote the manuscript with contributions from all other co-authors. The authors acknowledge Fei Teng, Tengfei Xu, Zhixiao Jiang, Siyu Chen and Chang Zhao (First Institute of Oceanography and Key Laboratory of Marine Sciences and Numerical Modelling, Ministry of Natural Resources, China) and Zhijian Li (School of Environment, Tsinghua University) for instruments maintenance during the round-the-world cruise.

Data availability

Data will be made available on request.

Declaration of competing interest

The authors declare that they have no conflict of interest.

Acknowledgement

National Natural Science Foundation for Outstanding Young Scholars (22222604).

Appendix A. Supplementary data

Supplementary data to this article can be found online at https://doi.org/10.1016/j.scitotenv.2023.164691.

References

Amos, H.M., Jacob, D.J., Streets, D.G., Sunderland, E.M., 2013. Legacy impacts of all-time anthropogenic emissions on the global mercury cycle: global impacts of legacy mercury. Glob. Biogeochem. Cycles 27, 410–421. https://doi.org/ https://doi.org/10.1002/gbc.20040.

Andersson, M.E., Gårdfeldt, K., Wängberg, I., Strömberg, D., 2008. Determination of Henry's law constant for elemental mercury. Chemosphere 73, 587–592. https://doi.org/ https://doi.org/10.1016/j.chemosphere.2008.05.067.

Angot, H., Barret, M., Magand, O., Ramonet, M., Dommergue, A., 2014. A 2-year record of atmospheric mercury species at a background Southern Hemisphere station on Amsterdam Island. Atmos. Chem. Phys. 14, 11461–11473. https://doi.org/ https://doi.org/10.5194/acp-14-11461-2014.

Angot, H., Dion, I., Vogel, N., Legrand, M., Magand, O., Dommergue, A., 2016. Multi-year record of atmospheric mercury at Dumont d'Urville, East Antarctic coast: continental outflow and oceanic influences. Atmos. Chem. Phys. 16, 8265–8279. https://doi.org/ https://doi.org/10.5194/acp-16-8265-2016.

Ariya, P.A., Amyot, M., Dastoor, A., Deeds, D., Feinberg, A., Kos, G., Poulain, A., Ryjkov, A., Semeniuk, K., Subir, M., Toyota, K., 2015. Mercury physicochemical and biogeochemical transformation in the atmosphere and at atmospheric interfaces: a review and future directions. Chem. Rev. 115, 3760–3802. https://doi.org/ https://doi.org/10.1021/cr500667e.

Behrenfeld, M.J., Falkowski, P.G., 1997. Photosynthetic rates derived from satellite-based chlorophyll concentration. Limnol. Oceanogr. 42, 1–20. https://doi.org/ https://doi.org/10.4319/lo.1997.42.1.0001.

Ci, Z., Wang, C., Wang, Z., Zhang, X., 2015. Elemental mercury (Hg(0)) in air and surface waters of the Yellow Sea during late spring and late fall 2012: concentration, spatial-temporal distribution and air/sea flux. Chemosphere 119, 199–208. https://doi.org/ https://doi.org/10.1016/j.chemosphere.2014.05.064.

Ci, Z.J., Zhang, X.S., Wang, Z.W., Niu, Z.C., Diao, X.Y., Wang, S.W., 2011. Distribution and air-sea exchange of mercury (Hg) in the Yellow Sea. Atmos. Chem. Phys. 11, 2881–2892. https://doi.org/ https://doi.org/10.5194/acp-11-2881-2011.

Diéguez, M.C., Bencardino, M., García, P.E., D'Amore, F., Castagna, J., De Simone, F., Soto Cárdenas, C., Ribeiro Guevara, S., Pirrone, N., Sprovieri, F., 2019. A multi-year record of atmospheric mercury species at a background mountain station in Andean Patagonia (Argentina): temporal trends and meteorological influence. Atmos. Environ. 214, 116819. https://doi.org/ https://doi.org/10.1016/j.atmosenv.2019.116819.

Dommergue, A., Ferrari, C.P., Gauchard, P.-A., Boutron, C.F., Poissant, L., Pilote, M., Jitaru, P., Adams, F.C., 2003. The fate of mercury species in a sub-arctic snowpack during snowmelt: fate of mercury species in a sub-Arctic snowpack during snowmelt. Geophys. Res. Lett. 30. https://doi.org/ https://doi.org/10.1029/2003GL017308.

Driscoll, C.T., Mason, R.P., Chan, H.M., Jacob, D.J., Pirrone, N., 2013. Mercury as a global pollutant: sources, pathways, and effects. Environ. Sci. Technol. 47, 4967–4983. https://doi.org/ https://doi.org/10.1021/es305071v.

Fleming, Z.L., Monks, P.S., Manning, A.J., 2012. Review: untangling the influence of air-mass history in interpreting observed atmospheric composition. Atmos. Res. 104–105, 1–39. https://doi.org/ https://doi.org/10.1016/j.atmosres.2011.09.009.

Fu, X.W., Zhang, H., Yu, B., Wang, X., Lin, C.-J., Feng, X.B., 2015. Observations of atmospheric mercury in China: a critical review. Atmos. Chem. Phys. 15, 9455–9476. https://doi.org/ https://doi.org/10.5194/acp-15-9455-2015.

Gustin, M.S., Bank, M.S., Bishop, K., Bowman, K., Branfireun, B., Chételat, J., Eckley, C.S., Hammerschmidt, C.R., Lamborg, C., Lyman, S., Martínez-Cortizas, A., Sommar, J., Tsui, M.T.-K., Zhang, T., 2020. Mercury biogeochemical cycling: a synthesis of recent scientific advances. Sci. Total Environ. 737, 139619. https://doi.org/ https://doi.org/10.1016/j.scitotenv.2020.139619.

Hu, C., Lee, Z., Franz, B., 2012. Chlorophyll a algorithms for oligotrophic oceans: a novel approach based on three-band reflectance difference: a novel ocean chlorophyll a algorithm. J. Geophys. Res. 117. https://doi.org/ https://doi.org/10.1029/2011JC007395.

Kalinchuk, V., Lopatnikov, E., Astakhov, A., 2018a. Gradient measurements of gaseous elemental mercury (Hg_0) in the marine boundary layer of the northwest Sea of Japan (East Sea). Environ. Pollut. 237, 1124–1136. https://doi.org/ https://doi.org/10.1016/j.envpol.2017.11.055.

Kalinchuk, V., Lopatnikov, E., Astakhov, A., 2018b. Gradient measurements of gaseous elemental mercury (Hg_0) in the marine boundary layer of the northwest Sea of Japan (East Sea). Environ. Pollut. 237, 1124–1136. https://doi.org/ https://doi.org/10.1016/j.envpol.2017.11.055.

Kalinchuk, V., Aksentov, K., Karnaukh, V., 2019. Gaseous elemental mercury (Hg(0)) in the surface air over the Sea of Japan, the Sea of Okhotsk and the Kuril-Kamchatka sector of the Pacific Ocean in August–September 2017. Chemosphere 224, 668–679. https://doi.org/ https://doi.org/10.1016/j.chemosphere.2019.02.185.

Koenig, A.M., Magand, O., Laj, P., Andrade, M., Moreno, I., Velarde, F., Salvatierra, G., Gutierrez, R., Blacutt, L., Aliaga, D., Reichler, T., Sellegri, K., Laurent, O., Ramonet, M., Dommergue, A., 2021. Seasonal patterns of atmospheric mercury in tropical South America as inferred by a continuous total gaseous mercury record at Chacaltaya station (5240 m) in Bolivia. Atmos. Chem. Phys. 21, 3447–3472. https://doi.org/ https://doi.org/10.5194/acp-21-3447-2021.

Kuss, J., Zülicke, C., Pohl, C., Schneider, B., 2011. Atlantic mercury emission determined from continuous analysis of the elemental mercury sea-air concentration difference within transects between 50°N and 50°S: Atlantic Hg sea-air concentration difference. Glob. Biogeochem. Cycles 25, n/a-n/a. https://doi.org/ https://doi.org/10.1029/2010GB003998.

Kuss, J., Wasmund, N., Nausch, G., Labrenz, M., 2015. Mercury emission by the Baltic Sea: a consequence of cyanobacterial activity, photochemistry, and low-light mercury transformation. Environ. Sci. Technol. 49, 11449–11457. https://doi.org/ https://doi.org/10.1021/acs.est.5b02204.

Lan, X., Talbot, R., Castro, M., Perry, K., Luke, W., 2012. Seasonal and diurnal variations of atmospheric mercury across the US determined from AMNet monitoring data. Atmos. Chem. Phys. 12, 10569–10582. https://doi.org/ https://doi.org/10.5194/acp-12-10569-2012.

Lyman, S.N., Cheng, I., Gratz, L.E., Weiss-Penzias, P., Zhang, L., 2020. An updated review of atmospheric mercury. Sci. Total Environ. 707, 135575. https://doi.org/ https://doi.org/10.1016/j.scitotenv.2019.135575.

Mao, H., Cheng, I., Zhang, L., 2016. Current understanding of the driving mechanisms for spatiotemporalvariations of atmospheric speciated mercury: a review. Atmos. Chem. Phys. 16, 12897–12924. https://doi.org/ https://doi.org/10.5194/acp-16-12897-2016.

Martin, L.G., Labuschagne, C., Brunke, E.-G., Weigelt, A., Ebinghaus, R., Slemr, F., 2017. Trend of atmospheric mercury concentrations at Cape Point for 1995–2004 and since 2007. Atmos. Chem. Phys. 17, 2393–2399. https://doi.org/ https://doi.org/10.5194/acp-17-2393-2017.

Nerentorp Mastromonaco, M., Gårdfeldt, K., Jourdain, B., Abrahamsson, K., Granfors, A., Ahnoff, M., Dommergue, A., Méjean, G., Jacobi, H.-W., 2016. Antarctic winter mercury and ozone depletion events over sea ice. Atmos. Environ. 129, 125–132. https://doi.org/ https://doi.org/10.1016/j.atmosenv.2016.01.023.

O'Driscoll, N.J., Siciliano, S.D., Lean, D.R.S., Amyot, M., 2006. Gross photoreduction kinetics of mercury in temperate freshwater lakes and rivers: application to a general model of DGM dynamics. Environ. Sci. Technol. 40, 837–843. https://doi.org/ https://doi.org/10.1021/es051062y.

Polissar, A.V., Hopke, P.K., Harris, J.M., 2001. Source regions for atmospheric aerosol measured at Barrow, Alaska. Environ. Sci. Technol. 35, 4214–4226. https://doi.org/ https://doi.org/10.1021/es0107529.

Qureshi, A., O'Driscoll, N.J., MacLeod, M., Neuhold, Y.-M., Hungerbühler, K., 2010. Photoreactions of mercury in surface ocean water: gross reaction kinetics and possible pathways. Environ. Sci. Technol. 44, 644–649. https://doi.org/ https://doi.org/10.1021/es9012728.

Rose, C.H., Ghosh, S., Blum, J.D., Bergquist, B.A., 2015. Effects of ultraviolet radiation on mercury isotope fractionation during photo-reduction for inorganic and organic mercury species. Chem. Geol. 405, 102–111. https://doi.org/ https://doi.org/10.1016/j.chemgeo.2015.02.025.

Siciliano, S.D., O'Driscoll, N.J., Lean, D.R.S., 2002. Microbial reduction and oxidation of mercury in freshwater lakes. Environ. Sci. Technol. 36, 3064–3068. https://doi.org/ https://doi.org/10.1021/es010774v.

Slemr, F., Angot, H., Dommergue, A., Magand, O., Barret, M., Weigelt, A., Ebinghaus, R., Brunke, E.-G., Pfaffhuber, K.A., Edwards, G., Howard, D., Powell, J., Keywood, M., Wang, F., 2015. Comparison of mercury concentrations measured at several sites in the southern hemisphere. Atmos. Chem. Phys. 15, 3125–3133. https://doi.org/ https://doi.org/10.5194/acp-15-3125-2015.

Soerensen, A.L., Mason, R.P., Balcom, P.H., Jacob, D.J., Zhang, Y., Kuss, J., Sunderland, E.M., 2014. Elemental mercury concentrations and fluxes in the tropical atmosphere and ocean. Environ. Sci. Technol. 48, 11312–11319. https://doi.org/ https://doi.org/10.1021/es503109p.

Sprovieri, F., Pirrone, N., Bencardino, M., D'Amore, F., Carbone, F., Cinnirella, S., Mannarino, V., Landis, M., Ebinghaus, R., Weigelt, A., Brunke, E.-G., Labuschagne, C., Martin, L., Munthe, J., Wängberg, I., Artaxo, P., Morais, F., Barbosa, H.M.J., Brito, J., Cairns, W., Barbante, C., Diéguez, M.C., Garcia, P.E., Dommergue, A., Angot, H., Magand, O., Skov, H., Horvat, M., Kotnik, J., Read, K.A., Neves, L.M., Gawlik, B.M., Sena, F., Mashyanov, N., Obolkin, V., Wip, D., Feng, X.B., Zhang, H., Fu, X., Ramachandran, R., Cossa, D., Knoery, J., Marusczak, N., Nerentorp, M., Norstrom, C., 2016. Atmospheric mercury concentrations observed at ground-based monitoring sites globally distributed in the framework of the GMOS network. Atmos. Chem. Phys. 16, 11915–11935. https://doi.org/ https://doi.org/10.5194/acp-16-11915-2016.

Stein, A.F., Draxler, R.R., Rolph, G.D., Stunder, B.J.B., Cohen, M.D., Ngan, F., 2015. NOAA's hysplit atmospheric transport and dispersion modeling system. Bull. Am. Meteorol. Soc. 96, 2059–2077. https://doi.org/ https://doi.org/10.1175/BAMS-D-14-00110.1.

Su, W., Charlock, T.P., Rose, F.G., 2005. Deriving surface ultraviolet radiation from Ceres surface and atmospheric radiation budget: methodology: deriving surface ultraviolet radiation from Ceres. J. Geophys. Res. 110, n/a-n/a. https://doi.org/ https://doi.org/10.1029/2005JD005794.

Tang, Y., Wang, S., Wu, Q., Liu, K., Wang, L., Li, S., Gao, W., Zhang, L., Zheng, H., Li, Z., Hao, J., 2018. Recent decrease trend of atmospheric mercury concentrations in East China: the influence of anthropogenic emissions. Atmos. Chem. Phys. 18, 8279–8291. https://doi.org/ https://doi.org/10.5194/acp-18-8279-2018.

Tseng, C.M., Liu, C.S., Lamborg, C., 2012. Seasonal changes in gaseous elemental mercury in relation to monsoon cycling over the northern South China Sea. Atmos. Chem. Phys. 12, 7341–7350. https://doi.org/ https://doi.org/10.5194/acp-12-7341-2012.

Wang, J., Zhang, L., Xie, Z., 2016. Total gaseous mercury along a transect from coastal to central Antarctic: spatial and diurnal variations. J. Hazard. Mater. 317, 362–372. https://doi.org/ https://doi.org/10.1016/j.jhazmat.2016.05.068.

Wang, J., Xie, Z., Wang, F., Kang, H., 2017. Gaseous elemental mercury in the marine boundary layer and air-sea flux in the Southern Ocean in austral summer. Sci. Total Environ. 603–604, 510–518. https://doi.org/ https://doi.org/10.1016/j.scitotenv.2017.06.120.

Wang, S., McNamara, S.M., Moore, C.W., Obrist, D., Steffen, A., Shepson, P.B., Staebler, R.M., Raso, A.R.W., Pratt, K.A., 2019. Direct detection of atmospheric atomic bromine leading to mercury and ozone depletion. Proc. Natl. Acad. Sci. U. S. A. 116, 14479–14484. https://doi.org/ https://doi.org/10.1073/pnas.1900613116.

Wang, Y., Wu, P., Zhang, Y., 2023. Climate-driven changes of global marine mercury cycles in 2100. Proc. Natl. Acad. Sci. U. S. A. 120, e2202488120. https://doi.org/ https://doi.org/10.1073/pnas.2202488120.

Weiss-Penzias, P.S., Williams, E.J., Lerner, B.M., Bates, T.S., Gaston, C., Prather, K., Vlasenko, A., Li, S.M., 2013. Shipboard measurements of gaseous elemental mercury along the coast of Central and Southern California J. Geophys. Res. Atmos. 118, 208–219. https://doi.org/ https://doi.org/10.1029/2012JD018463.

Williamson, C.E., Zepp, R.G., Lucas, R.M., Madronich, S., Austin, A.T., Ballaré, C.L., Norval, M., Sulzberger, B., Bais, A.F., McKenzie, R.L., Robinson, S.A., Häder, D.-P., Paul, N.D., Bornman, J.F., 2014. Solar ultraviolet radiation in a changing climate. Nat. Clim. Change 4, 434–441. https://doi.org/ https://doi.org/10.1038/nclimate2225.

Yang, X., Jiskra, M., Sonke, J.E., 2019. Experimental rainwater divalent mercury speciation and photoreduction rates in the presence of halides and organic carbon. Sci. Total Environ. 697, 133821. https://doi.org/ https://doi.org/10.1016/j.scitotenv.2019.133821.

Yue, F., Xie, Z., Yan, J., Zhang, Y., Jiang, B., 2021. Spatial distribution of atmospheric mercury species in the Southern Ocean. Geophys. Res. Atmos. 126. https://doi.org/ https://doi.org/10.1029/2021JD034651.

Yue, F., Xie, Z., Zhang, Y., Yan, J., Zhao, S., 2022. Latitudinal distribution of gaseous elemental mercury in tropical Western Pacific: the role of the doldrums and the ITCZ. Environ. Sci. Technol. 56, 2968–2976. https://doi.org/ https://doi.org/10.1021/acs.est.1c07229.

Zhang, Y., Jacob, D.J., Horowitz, H.M., Chen, L., Amos, H.M., Krabbenhoft, D.P., Slemr, F., St. Louis, V.L., Sunderland, E.M., 2016. Observed decrease in atmospheric mercury explained by global decline in anthropogenic emissions. Proc. Natl. Acad. Sci. U. S. A. 113, 526–531. https://doi.org/ https://doi.org/10.1073/pnas.1516312113.

Zhang, Y., Horowitz, H., Wang, J., Xie, Z., Kuss, J., Soerensen, A.L., 2019. A coupled global atmosphere-ocean model for air-sea exchange of mercury: insights into wet deposition and atmospheric redox chemistry. Environ. Sci. Technol. 53, 5052–5061. https://doi.org/ https://doi.org/10.1021/acs.est.8b06205.

Zheng, X., Cheng, H., 2020. Comparison of solar ultraviolet irradiance measurements at Zhongshan Station, Antarctica. J. Appl. Meteorol. Sci. 31. https://doi.org/10.11898/1001-7313.20200410.